Langmuir

Article

pubs.acs.org/Langmuir

Photoactivation and Saturated Emission in Blended Conjugated Polymer Nanoparticles

Xiaoli Wang, Louis C. Groff, and Jason D. McNeill*

Department of Chemistry, Clemson University, Clemson, South Carolina 29634, United States

Supporting Information

ABSTRACT: Blended poly[(9,9-dioctylfluorenyl-2,7-diyl)-*co*-(1,4-benzo-{2,1′,3}-thiadiazole)] (PFBT)/poly[2-methoxy-5-(2-ethylhexyloxy)-1,4-phenylenevinylene] (MEH-PPV) conjugated polymer nanoparticles were prepared and characterized by conventional and single-particle fluorescence spectroscopy. The particles exhibit red emission and improved quantum efficiency resulting from highly efficient energy transfer from donor PFBT to acceptor MEH-PPV as well as suppression of MEH-PPV aggregation. Photobleaching results indicate better photostability in the blended sample compared to undoped MEH-PPV nanoparticles and photoactivation of donor emission, which could be useful for single-molecule localization-based super-resolution microscopy. Single blended nanoparticles exhibit bright fluorescence as well as saturation behavior at very low excitation intensities. These and other properties of the blended conjugated polymer nanoparticles could provide substantial improvements in resolution when employed in super-resolution microscopy.

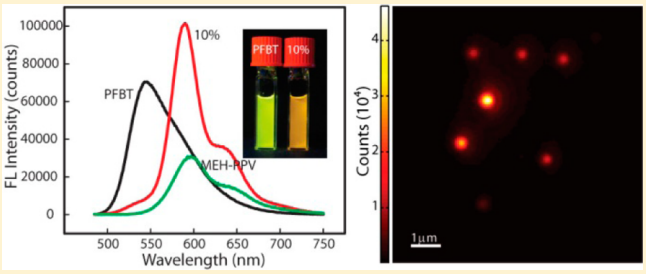

INTRODUCTION

There is current interest in the development of brighter, nanoparticle-based fluorescent probes for a variety of applications. Conjugated polymer nanoparticles (CPNs) have emerged as a promising class of fluorescent nanoparticles,[1,2] with higher brightness than similar-sized dye-loaded silica nanoparticles[3] and colloidal semiconductor quantum dots.[4] CPNs have been demonstrated in a number of fluorescence-based applications, such as sensors,[5,6] photoswitching nanoparticles,[7] and in vivo imaging.[8] Similarly, conjugated polyelectrolytes exhibit high brightness and have been demonstrated in several solution-based sensing applications.[9−11] CPNs made of polyfluorene derivative poly[(9,9-dioctylfluorenyl-2,7-diyl)-*co*-(1,4-benzo-{2,1′,3}-thiadiazole)] (PFBT)[12] have exhibited excellent figures of merit for several different applications, such as nanometer resolution particle tracking[13] and cellular imaging.[14]

There is interest in the development CPNs with red-shifted emission spectra, which could help reduce background due to scattering and autofluorescence.[15] We had previously explored the possibility of employing energy transfer to dyes and blending with other conjugated polymers to red-shift the emission.[16,17] However, the polyfluorene host polymer used previously requires excitation in the near UV, which is not convenient for laser excitation, and autofluorescence can be a problem for excitation in this wavelength range.[15] Here, we employed a strategy of using PFBT as the host polymer, preparing nanoparticles blended with a small amount of poly[2-methoxy-5-(2-ethylhexyloxy)-1,4-phenylenevinylene] (MEH-PPV), based on the notion that energy transfer from PFBT to MEH-PPV would result in red-shifted emission, whereas the small molecule fraction of MEH-PPV would limit aggregation-induced quenching typically observed in MEHPPV.[18,19] The fluorescence spectra show highly efficient energy transfer from the donor polymer (PFBT) to the acceptor polymer (MEH-PPV) as well as significantly improved quantum yield as compared to unblended MEH-PPV nanoparticles.

Here, we also explore the optical properties of blended PFBT:MEH-PPV CPNs that are important for some super-resolution fluorescence-based imaging techniques. The resolution obtained using various super-resolution fluorescence imaging techniques such as PALM, RESOLFT, and related methods is often dependent on the optical properties of the chromophores employed, including saturation and photoswitching behavior.[20,21] Ideally, chromophores for saturation-based methods should have a high emission rate at saturation and exhibit saturation at low excitation intensities. The small organic dye molecules typically employed for saturation-based imaging involve trade-offs with respect to maximizing signal level and minimizing photodamage. Small organic dye molecules with low triplet yields exhibit high triplet-saturated emission (on the order of 10^7 s^{-1})[22] but require moderate-to-high excitation intensities (e.g., 10^4−10^5 W/cm^2), which can cause photodamage, whereas dyes with higher triplet yields exhibit saturation at lower excitation intensities but exhibit reduced emission rates. However, PFBT nanoparticles exhibit significantly higher saturated emission rates (~10^8 s^{-1}) at significantly lower excitation intensities (~500 W/cm^2).[23]

Received: July 25, 2013
Revised: September 27, 2013
Published: October 7, 2013

Typical photoactivated chromophores used in tracking and localization microscopy techniques emit on the order of 10^5 photons prior to photobleaching, which limits the localization accuracy and thus the resolution,[24,25] whereas PFBT nanoparticles emit ~10^9 photons prior to photobleaching, resulting in a localization uncertainty of better than 1 nm.[13] For the blended PFBT:MEH-PPV nanoparticles, we determine extraordinary figures of merit for photoactivation and saturation-based imaging, significantly better than those obtained for unblended PFBT CPNs. The results indicate that the improved figures of merit derive from a combination of factors, including the high fluorescence brightness of the polymers employed, highly efficient exciton funneling from the host to the dopant polymer, and quenching by photogenerated polarons.

EXPERIMENTAL SECTION

Materials. The copolymer poly[(9,9-dioctylfluorenyl-2,7-diyl)-*co*-(1,4-benzo-{2,1′,3}-thiadiazole)] (PFBT, MW 10,000, polydispersity = 1.7) and the poly(phenylene vinylene) derivative poly[2-methoxy-5-(2-ethylhexyloxy)-1,4-phenylenevinylene] (MEH-PPV, MW 200,000, polydispersity = 4.0) were purchased from ADS Dyes, Inc. (Quebec, Canada). Fluorescein (reference standard) was purchased from Life Technologies (Invitrogen). The solvent tetrahydrofuran (THF, anhydrous, 99.9%), 3-aminopropyl trimethoxysilane (APS, 97%), and sodium hydroxide (NaOH, SigmaUltra, minimum 98%) were purchased from Sigma-Aldrich (Milwaukee, WI). All chemicals were used as provided without further purification.

Preparation of Nanoparticles. Conjugated polymer nanoparticles were prepared by a nanoprecipitation procedure, described previously.[17] Briefly, 1000 ppm stock solutions of PFBT and MEH-PPV in THF were prepared by dissolving PFBT or MEH-PPV in THF by stirring, and the resulting solutions were then filtered through a 0.45 μm membrane filter (Millipore). The solutions were then diluted to 20 ppm. For blended nanoparticles, the polymer solutions were mixed in accordance with the desired weight ratio. Then, 2 mL of each solution was rapidly injected into 8 mL of water under sonication. The THF solvent was removed by heating to 40 °C under N_2 flow, and the nanoparticle suspension was filtered through a 0.1 μm membrane filter to remove aggregates. The resulting CPN suspensions were clear and colloidally stable for several months, with no changes in spectroscopic characteristics.

Characterization. The size distribution was determined by atomic force microscopy (AFM). For AFM measurement, the samples were prepared by drop-casting onto APS functionalized glass coverslips. After evaporation of water, the surface topography was imaged with an Ambios Q250 multimode AFM in AC mode. UV−vis spectra were obtained using a Shimadzu UV-2101 PC scanning spectrophotometer with 1 cm quartz cuvettes. Fluorescence spectra were recorded with a commercial fluorometer (Quantamaster, PTI, Inc.). Photobleaching experiments were conducted using a custom fluorometer in which a 473 nm beam from a diode-pumped solid-state (DPSS) continuous wave blue laser was employed as the excitation source and a CCD spectrograph ($^1/_8$ m monochromator, Acton; Spec-10 CCD, Princeton Instruments) was used as detector. A 1 cm cuvette with 0.8 mL of the nanoparticle suspension was illuminated with 18 mW laser excitation intensity under stirring for a total of 2 h, acquiring a spectrum every 0.5 s.

For single-nanoparticle measurements, a sample coverslip was prepared using the same method as used for preparing the sample for AFM, as described above. Measurements were performed on a custom epifluorescence microscope. The 473 nm excitation laser was coupled via optical fiber to the rear epi port of an inverted fluorescence microscope (Olympus IX-71). A 500 nm dichroic (Chroma 500 DCLP) was used to direct the beam into a high numerical aperture objective (Olympus Ach, 100×, 1.25 NA, Oil). The laser excitation at the sample plane exhibits a Gaussian profile with fwhm of ~3 μm, and the typical laser intensities employed ranged from ~10 to ~2000 W/cm^2 in the center of the laser spot, depending on the experiment. Fluorescence from the nanoparticles was collected by the same objective and filtered through a 500 nm long-pass filter and then focused onto an sCMOS camera (Neo sCMOS, Andor) resulting in a pixel resolution of 65 nm/pixel. For typical photobleaching kinetics measurements, an acquisition time of 0.5 s per frame with total acquisition duration of ~250 s was employed to ensure >95% photobleaching by the end of the acquisition. For single-nanoparticle fluorescence saturation measurements, a series of excitation intensities was used to excite the sample, and the corresponding fluorescence images were recorded.

RESULTS AND DISCUSSION

To obtain brighter CPNs with red-shifted emission spectra, we employed a Förster resonance energy transfer (FRET) strategy. Figure 1a shows the chemical structures of polymers that were

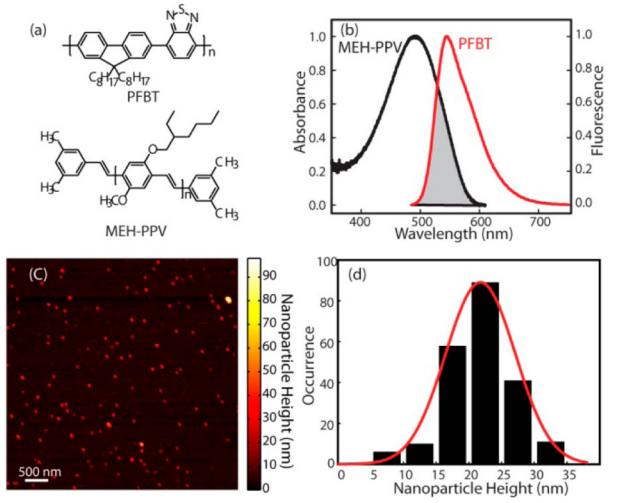

Figure 1. (a) Chemical structures of conjugated polymers PFBT and MEH-PPV; (b) spectral overlap between absorption spectrum of MEH-PPV in THF and emission spectrum of PFBT CPNs; (c) representative AFM image of PFBT nanoparticles; (d) histogram of PFBT nanoparticle height.

used. PFBT was chosen as the host polymer because of its high photostability and high brightness for fluorescence microscopy.[23] MEH-PPV was employed for dopant polymer due to its red emission spectrum, high absorptivity (peak extinction coefficient = 1.5 × 10^7 M^{-1} cm^{-1} for a molecular weight of 200,000), and good spectral overlap with the emission spectrum of PFBT (shown in Figure 1b), which facilitates efficient energy transfer. The nanoparticle suspensions were immobilized on a glass coverslip for analysis of particle morphology and size distribution by AFM. Panels c and d of Figure 1 show a representative AFM image and the particle height histogram of undoped PFBT nanoparticles, respectively. The particle size was determined to be 22 ± 5 nm. The presence of the dopant polymer MEH-PPV has no apparent effect on particle morphology and size distribution.

Optical Properties. UV−vis spectra for 10% blended CPNs (Figure 2a) exhibit an absorption peak of ~456 nm, which is consistent with the host polymer PFBT, and a small absorption bump at ~560 nm (in circle) from the dopant polymer MEH-PPV. The relative size of the PFBT and MEH-PPV features in the UV−vis spectrum is roughly consistent with their extinction properties and the mass ratio of the two polymers. The inset in Figure 2a is a photograph of sample PFBT CPNs and 10% PFBT/MEH-PPV CPNs suspensions

dx.doi.org/10.1021/la402767j | Langmuir 2013, 29, 13925−13931

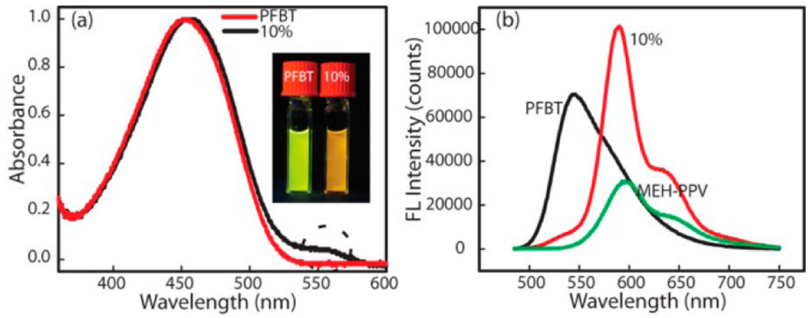

Figure 2. (a) Normalized UV−vis absorption spectrum of PFBT and 10% PFBT/MEH-PPV nanoparticles (inset, picture of PFBT and 10% PFBT/MEH-PPV sample under UV lamp); (b) fluorescence spectra of polymer nanoparticles PFBT, 10% PFBT/MEH-PPV, and MEH-PPV under λ_{ex} = 473 nm.

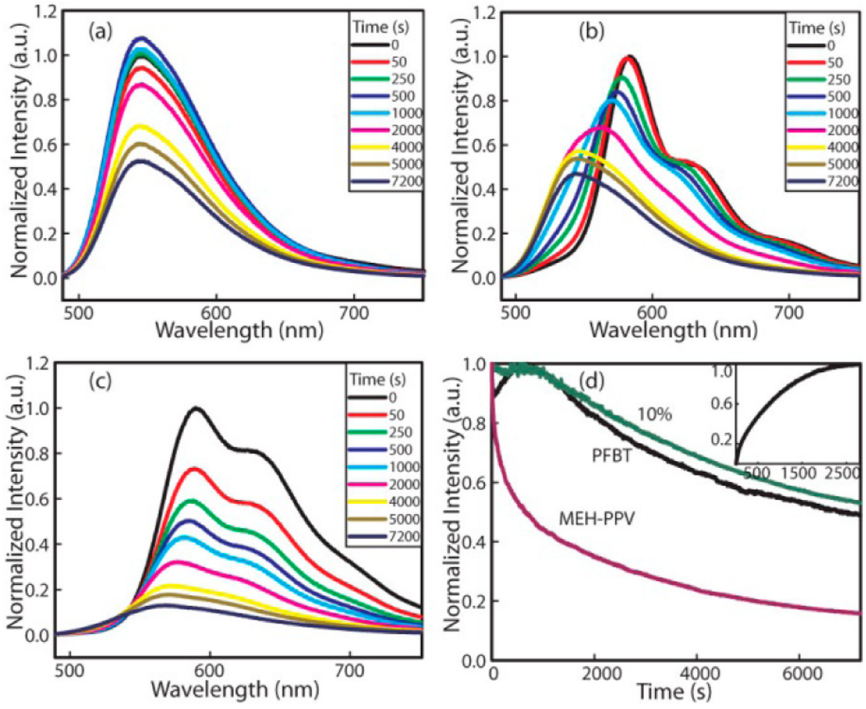

Figure 3. (a−c) Time evolution of fluorescence emission spectra during photobleaching of PFBT, 10% PFBT/MEH-PPV, and MEH-PPV CPNs; (d) photobleaching decay curves of PFBT, 10% PFBT/MEH-PPV, and MEH-PPV CPNs (inset, photoactivation of donor PFBT emission in blended CPNs).

under UV lamp illumination (365 nm). The color change from yellow-green to orange emission indicates highly efficient energy transfer between PFBT and MEH-PPV.

The fluorescence spectra shown in Figure 2b clearly indicate efficient energy transfer. At 10% dopant concentration, ∼90% of the PFBT fluorescence is quenched, indicating an energy transfer efficiency of ∼90%,[17] and the MEH-PPV peak predominates. The fluorescence quantum yield of 10% blended CPNs is the same as that of undoped PFBT nanoparticles (13%) and much higher than that of undoped MEH-PPV nanoparticles (5%). The MEH-PPV peak in blended CPNs is around 590 nm and slightly blue-shifted compared to undoped MEH-PPV nanoparticles, where the peak is ∼597 nm. The increased quantum yield and slightly blue-shifted spectrum is consistent with our initial hypothesis that blending with PFBT would reduce aggregation quenching of MEH-PPV.

The fact that the fluorescence yield for undoped PFBT nanoparticles is the same as for the blended particles raises the question of whether this result is coincidental or perhaps indicates some important underlying principle or relationship. On the basis of previous results, it appears that the lifetime of the PFBT excited state and the fluorescence quantum yield are largely determined by the radiative rate and quenching via a dynamic quenching process.[26] If this holds, then energy transfer to the acceptor polymer would compete with both the quenching process and emission from the donor. If the fluorescence quantum yield of the acceptor is higher than that of the donor, this would result in a higher quantum yield for the blended nanoparticle than for nanoparticles containing only the host/donor polymer. However, this is not observed in the present case, indicating that either the MEH-PPV in the blended CPNs has a quantum yield similar to that of the PFBT donor or that the quenching process that largely determines the quantum yield of PFBT is a static process or that the quenching process affects both MEH-PPV and PFBT equally. Additional experiments and analysis are needed to answer this question definitively.

dx.doi.org/10.1021/la402767j | *Langmuir* 2013, 29, 13925−13931

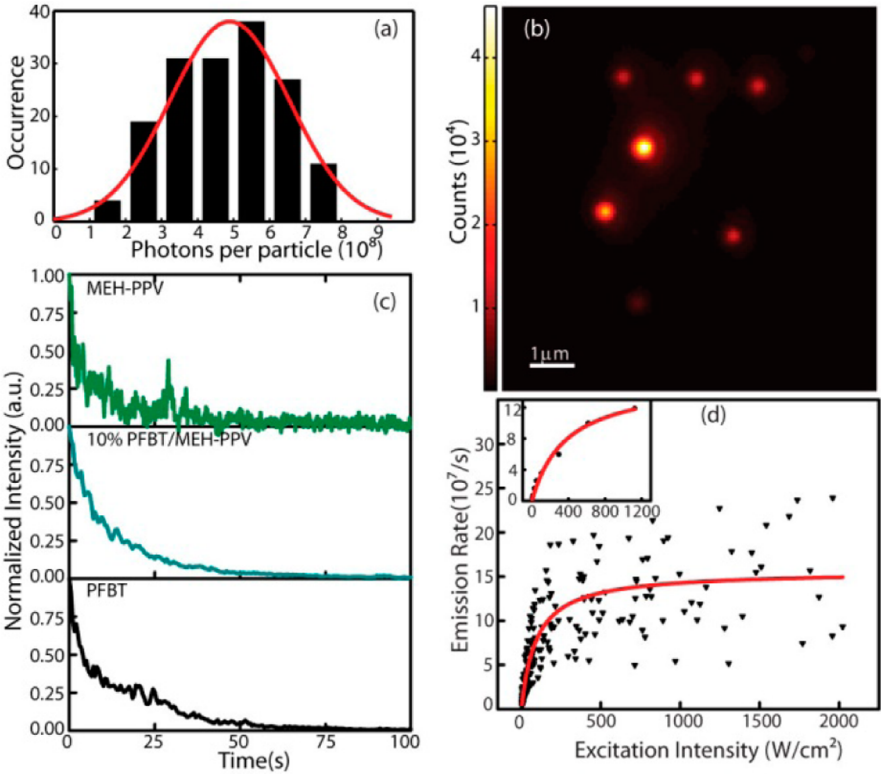

Figure 4. (a) Histogram of emitted photon numbers of individual 10% PFBT/MEH-PPV nanoparticles prior to irreversible photobleaching; (b) representative fluorescence image of single 10% PFBT/MEH-PPV nanoparticles immobilized on a coverslip; (c) typical photobleaching trajectories of single PFBT, 10% PFBT/MEH-PPV, and MEH-PPV nanoparticle; (d) fluorescence saturation of single 10% PFBT/MEH-PPV nanoparticles with increasing excitation intensity (the scattered points are the experimental data for several particles, whereas the solid red curve represents a fit to the saturation equation $R = R_\infty(I_e/I_s)(1 + I_e/I_s)^{-1}$; inset, a typical single nanoparticle saturation curve).

Photostability. Photostability (resistance to photobleaching) is a key characteristic of fluorescent nanoparticles for high-speed particle tracking as well as for long-term imaging studies. Quantitative bulk photobleaching measurements were performed using undoped PFBT, 10% blended PFBT/MEH-PPV, and undoped MEH-PPV CPNs using a custom CCD-based fluorometer. The samples were illuminated under 473 nm laser while recording the fluorescence spectrum continuously over a period of 2 h (Figure 3). As the 10% blended CPNs photobleach, the MEH-PPV peak steadily decreases in intensity and shifts slightly toward the blue, whereas the PFBT peak steadily increases (Figure 4b). The decrease of the MEH-PPV peak and increase of the PFBT peak over time are attributed to decreased energy transfer as the acceptor is photobleached, as often occurs in systems undergoing FRET.[27] Integrating over the entire emission spectrum, the photobleaching lifetimes were determined to be 1.7×10^4, 1.9×10^4, and 5.4×10^3 s for PFBT, 10% PFBT/MEH-PPV, and MEH-PPV nanoparticles, respectively (fitting and analysis procedure details provided in the Supporting Information). The slight increase in photobleaching lifetime of 10% blended CPNs compared to undoped PFBT is not significant, but could indicate that the reduced lifetime of the donor excited state possibly reduces the photobleaching rate of the donor. The ratio between fluorescence quantum yield (ϕ_f) and photobleaching quantum yield (ϕ_{pb}) produces the average number of photons emitted per particle prior to photobleaching (here referred to as the photon number).[28] The results show the 10% blended sample emitted $\sim 4.2 \times 10^7$ photons (per particle), similar to the photon number of the PFBT sample (3.9×10^7) and ~25 times larger than undoped MEH-PPV nanoparticles (1.6×10^6).

Clearly, the blended nanoparticles exhibit increased fluorescence quantum yield, photon number, and photobleaching lifetime as compared to undoped MEH-PPV nanoparticles. Most of the improvement in photon number and photobleaching lifetime is due to the emission of the highly photostable PFBT polymer, because after ~4000 s, only PFBT fluorescence persists for the blended nanoparticles, as is evident in the spectrum at $t = 4000$ s (Figure 3b). However, the above analysis of the photobleaching dynamics of the integrated spectrum does not indicate whether MEH-PPV is more photostable in blended nanoparticles as compared to undoped MEH-PPV nanoparticles. Differences in photostability could result if, for example, aggregate species are more readily oxidized or are involved in promoting photo-oxidation or if the PFBT host acts as a quencher for radical, triplet, or other species involved in photobleaching. To pursue this question, we performed decomposition of the photobleaching spectra to determine the photobleaching rate constants of each component. The decomposition was somewhat problematic, because the position and shape of the MEH-PPV feature change somewhat over the course of the photobleaching experiment, which could lead to some artifacts in the decomposed kinetics trace, so the decomposed kinetics results are not definitive. The details of the decomposition are shown in the Supporting Information. After decomposition, the photobleaching curve of the MEH-PPV component exhibits a single exponential decay with a photobleaching time constant of 1260 s (Figure S3a in the Supporting Information). There is

dx.doi.org/10.1021/la402767j | Langmuir 2013, 29, 13925−13931

Table 1. Photostability Experiment Results[a]

sample	quantum yield (ϕ_f)	extinction coefficient (ε, $M^{-1}cm^{-1}$)	photobleaching lifetime τ_{av} (s)	photobleaching quantum yield (ϕ_{pb})	photon number (ϕ_f/ϕ_{pb})
PFBT	0.13	1.5×10^8	1.7×10^4	3.4×10^{-9}	3.9×10^7
10% PFBT/MEH-PPV	0.13		1.9×10^4	3.1×10^{-9}	4.2×10^7
MEH-PPV	0.05	4.5×10^7	5.4×10^3	3.1×10^{-8}	1.6×10^6

[a]All parameters are obtained at λ = 473 nm. Quantum yields were determined using fluorescein in 0.01 M NaOH as standard.

only 10% MEH-PPV in the blended CPNs, whereas the photobleaching lifetime of MEH-PPV component is ~20% that of undoped MEH-PPV CPNs. Energy transfer must be taken into account, because, in the case of the blended particles, the PFBT host effectively funnels energy to a relatively small number of MEH-PPV molecules, effectively increasing the excitation rate on a per-molecule basis, whereas in the case of undoped MEH-PPV particles, a similar number of excitations is distributed over a larger number of molecules. With this taken into account, the results suggest (assuming that the decomposition is sufficiently valid) that the MEH-PPV in blended CPNs is significantly more photostable than that in undoped MEH-PPV nanoparticles. Furthermore, in the undoped MEH-PPV photobleaching decay trace, the fluorescence emission dropped 20% in <40 s at the beginning of the experiment. This fast decay process likely involves quenching by photogenerated hole polarons,[26] whereas in the blended CPNs, the absence of this fast decay suggests that quenching by photogenerated polarons is suppressed. However, this analysis should be taken as speculative, because the spectral decomposition process could have introduced artifacts.

The PFBT fluorescence exhibits photoactivation phenomena, owing to acceptor photobleaching.[27] The PFBT component intensity increases steadily until around 2700 s, after which it starts decreasing, with a decay trace similar to that of undoped PFBT nanoparticles (Figure S3b in the Supporting Information). After fitting PFBT component decay trace (Figure S3c in the Supporting Information), the photoactivation time constant of PFBT in blended CPNs is determined to be 760 s, and on the basis of the excitation intensity, the number of excitation photons needed to activate PFBT fluorescence emission for a particle is 1.9×10^7. This photoactivation phenomenon could be useful for some super-resolution imaging applications. For instance, it could be used for differentiating particles that are too close to resolve in space, but experience different excitation intensities due to nonuniform illumination and, thus, "turn on" at different times. Similarly, due to particle-to-particle variation of the amount of MEH-PPV in blended CPNs, the photoactivation time of PFBT may differ between particles, even for uniform illumination. As such, the closely spaced nanoparticles could be resolved temporally.

Single-Nanoparticle Photobleaching and Saturation. To explore the properties of CPNs as fluorescent imaging probes, we performed single nanoparticle fluorescence imaging and kinetics measurements in air with a custom-built widefield epifluorescence microscope equipped with an sCMOS camera. Single-nanoparticle photobleaching kinetics experiments were performed by acquiring a series of consecutive image frames. The number of photons emitted by individual nanoparticles (here referred to as the photon number) was obtained from the sCMOS images with a custom-written script for MATLAB (Mathworks, Natick, MA) that integrates the intensity over each fluorescence spot in the sCMOS image and corrects for the gain factor (ADC counts per detected photon) and ADC offset, as well as takes into account the collection efficiency of the microscope and the detection efficiency of the detector.

The representative fluorescence image and death number histogram of 10% PFBT/MEH-PPV are shown in Figure 4a,b. The average photon numbers for different samples are given in Table 1. The photon number of undoped PFBT nanoparticles

Table 2. Single-Nanoparticle Experiment Results

sample	photon number	I_s (W/cm^2)	R_∞ (10^7photons/s)
PFBT	6.3×10^8	146	15.9
10% PFBT/MEH-PPV	4.9×10^8	94	15.6
MEH-PPV	1.4×10^7		

is consistent with the number reported previously.[23] The photon number of blended 10% PFBT/MEH-PPV nanoparticles is 4.9×10^8, which is close to that of the undoped PFBT CPNs (6.3×10^8) and 35 times larger than the number of undoped MEH-PPV CPNs (1.4×10^7). The slight discrepancy between the photon number from single-nanoparticle measurements and ensemble photobleaching experiments is likely caused by the combined effect of small calibration errors or differences in the experimental conditions, such as the aqueous environment in ensemble measurements, which could increase the availability of oxygen.[26] Typical single-nanoparticle photobleaching trajectories are presented in Figure 4c. Undoped MEH-PPV CPNs exhibit pronounced fluctuations or photoblinking behavior, whetrsd undoped PFBT and 10% PFBT/MEH-PPV exhibit a relatively continuous photobleaching curve.

Fluorescence saturation, a phenomenon in which fluorescence intensity plateaus as the excitation intensity increases, is a key process limiting the emission rate of fluorophores. Saturation phenomena can also be exploited for super-resolution imaging.[29] Saturation is typically caused by photogeneration of triplet states or other metastable "dark" states. For example, triplet saturation occurs when a substantial fraction of the molecules are in a long-lived, dark (nonfluorescent) triplet state, which occurs at high excitation intensity. For triplet saturation, the fluorescence intensity is given by

$$R = R_\infty \frac{I_e/I_s}{1 + I_e/I_s} \quad (1)$$

where R and R_∞ represent the actual emission rate and the saturation emission rate and I_e and I_s are the excitation intensity and the saturation intensity, respectively. The saturation phenomenon observed in CPNs is more complex, involving exciton diffusion, energy transfer, and quenching by photogenerated hole polarons, as shown previously.[2]

To experimentally determine saturation parameters of blended PFBT/MEH-PPV CPNs, we used a series of different

dx.doi.org/10.1021/la402767j | Langmuir 2013, 29, 13925−13931

excitation intensities (ranging from 10 to 2000 W/cm^2, starting at low intensity) to excite the sample and obtain a series of images. We purged the sample chamber with nitrogen to minimize photobleaching during experiments. The fluorescence emission rates of individual particles were extracted from the imaging data using a custom written MATLAB script, and the excitation intensity for every single nanoparticle was calculated on the basis of the Gaussian shape of the laser spot (3 μm fwhm) at the sample plane, together with the transmission efficiency of the objective (10%), determined previously. The emission rates versus excitation intensity are plotted and fit to obtain the saturation emission rate and saturation intensity. The saturation plot for 29 particles of 10% PFBT/MEH-PPV is shown in Figure 4d, and the inset is the saturation plot for a typical single nanoparticle. The wide range of saturation emission rates is likely due to the nanoparticle size distribution and the Poisson distribution of MEH-PPV chains per particle. By fitting to the (triplet) saturation equation (eq 1), the resulting average saturation emission rate, $R_\infty = 1.56 \times 10^8$ s^{-1}, is larger than the saturated emission rate of most dyes, and the average saturation intensity, $I_s = 94$ W/cm^2, is much lower than that of typical dyes. The saturation intensity is also significantly lower than that of undoped PFBT nanoparticles (shown in Table 1), which suggests that exciton funneling to the MEH-PPV dopant is involved. The combination of the relatively low saturation (excitation) intensity and high saturation emission rate is unparalleled and is favorable for saturation-based fluorescence imaging.[30] Another unusual property of the nanoparticles is the high particle-to-particle variation in the saturation excitation intensity, which varies from roughly 40 to 300 W/cm^2. This particle-to-particle saturation intensity variation could be useful for localizing positions of particles that are too close to spatially resolve by conventional fluorescence microscopy. By acquiring images at different excitation intensities, and calculating difference images, the particles saturated at lower intensities can be removed, and only the particles which have higher saturation intensities would be left in the images, and a similar differencing procedure could be used to select and determine positions of particles with low or intermediate saturation intensities.

In conclusion, we prepared blended PFBT/MEH-PPV CPNs that exhibit highly efficient energy transfer between donor PFBT and acceptor MEH-PPV. The blended polymer nanoparticles also exhibit improved photostability compared to undoped MEH-PPV nanoparticles. Single-nanoparticle imaging experiments indicate significantly improved figures of merit of PFBT:MEH-PPV CPNs as compared to dyes or unblended CPNs for advanced fluorescence-based imaging applications, including super-resolution fluorescence microscopy. These applications are currently under investigation.

■ ASSOCIATED CONTENT

Supporting Information

Full details of fluorescence quantum yield determination, saturation intensity and saturated emission rate and photobleaching lifetime calculation. This material is available free of charge via the Internet at http://pubs.acs.org.

■ AUTHOR INFORMATION

Corresponding Author

*(J.D.M.) E-mail: mcneill@clemson.edu.

Notes

The authors declare no competing financial interest.

■ ACKNOWLEDGMENTS

The authors acknowledge financial support from the NSF under Grant CHE-1058885.

■ REFERENCES

(1) Pecher, J.; Mecking, S. Nanoparticles of Conjugated Polymers. *Chem. Rev.* **2010**, *110*, 6260−6279.
(2) Wu, C. F.; Chiu, D. T. Highly Fluorescent Semiconducting Polymer Dots for Biology and Medicine. *Angew. Chem., Int. Ed.* **2013**, *52*, 3086−3109.
(3) Burns, A.; Ow, H.; Wiesner, U. Fluorescent Core-Shell Silica Nanoparticles: towards "Lab on a Particle" Architectures for Nanobiotechnology. *Chem. Soc. Rev.* **2006**, *35*, 1028−1042.
(4) Michalet, X.; Pinaud, F. F.; Bentolila, L. A.; Tsay, J. M.; Doose, S.; Li, J. J.; Sundaresan, G.; Wu, A. M.; Gambhir, S. S.; Weiss, S. Quantum Dots for Live Cells, in Vivo Imaging, and Diagnostics. *Science* **2005**, *307*, 538−544.
(5) Childress, E. S.; Roberts, C. A.; Sherwood, D. Y.; LeGuyader, C. L. M.; Harbron, E. J. Ratiometric Fluorescence Detection of Mercury Ions in Water by Conjugated Polymer Nanoparticles. *Anal. Chem.* **2012**, *84*, 1235−1239.
(6) Cordovilla, C.; Swager, T. M. Strain Release in Organic Photonic Nanoparticles for Protease Sensing. *J. Am. Chem. Soc.* **2012**, *134*, 6932−6935.
(7) Harbron, E. J.; Davis, C. M.; Campbell, J. K.; Allred, R. M.; Kovary, M. T.; Economou, N. J. Photochromic Dye-Doped Conjugated Polymer Nanoparticles: Photomodulated Emission and Nanoenvironmental Characterization. *J. Phys. Chem. C* **2009**, *113*, 13707−13714.
(8) Kim, S.; Lim, C. K.; Na, J.; Lee, Y. D.; Kim, K.; Choi, K.; Leary, J. F.; Kwon, I. C. Conjugated Polymer Nanoparticles for Biomedical in Vivo Imaging. *Chem. Commun.* **2010**, *46*, 1617−1619.
(9) Chen, L. H.; McBranch, D. W.; Wang, H. L.; Helgeson, R.; Wudl, F.; Whitten, D. G. Highly Sensitive Biological and Chemical Sensors based on Reversible Fluorescence Quenching in a Conjugated Polymer. *Proc. Natl. Acad. Sci. U.S.A.* **1999**, *96*, 12287−12292.
(10) Kumaraswamy, S.; Bergstedt, T.; Shi, X. B.; Rininsland, F.; Kushon, S.; Xia, W. S.; Ley, K.; Achyuthan, K.; McBranch, D.; Whitten, D. Fluorescent-Conjugated Polymer Superquenching Facilitates Highly Sensitive Detection of Proteases. *Proc. Natl. Acad. Sci. U.S.A.* **2004**, *101*, 7511−7515.
(11) Achyuthan, K. E.; Bergstedt, T. S.; Chen, L.; Jones, R. M.; Kumaraswamy, S.; Kushon, S. A.; Ley, K. D.; Lu, L.; McBranch, D.; Mukundan, H.; Rininsland, F.; Shi, X.; Xia, W.; Whitten, D. G. Fluorescence Superquenching of Conjugated Polyelectrolytes: Applications for Biosensing and Drug Discovery. *J. Mater. Chem.* **2005**, *15*, 2648−2656.
(12) Liu, B.; Bazan, G. C. Synthesis of Cationic Conjugated Polymers for Use in Label-Free DNA Microarrays. *Nat. Protoc.* **2006**, *1*, 1698−1702.
(13) Yu, J. B.; Wu, C. F.; Sahu, S. P.; Fernando, L. P.; Szymanski, C.; McNeill, J. D. Nanoscale 3D Tracking with Conjugated Polymer Nanoparticles. *J. Am. Chem. Soc.* **2009**, *131*, 18410−18414.
(14) Wu, C. F.; Schneider, T.; Zeigler, M.; Yu, J. B.; Schiro, P. G.; Burnham, D. R.; McNeill, J. D.; Chiu, D. T. Bioconjugation of Ultrabright Semiconducting Polymer Dots for Specific Cellular Targeting. *J. Am. Chem. Soc.* **2010**, *132*, 15410−15417.
(15) Rost, F. W. D. *Fluorescence Microscopy*, 1st ed.; Cambridge University Press: Cambridge, UK, 1992; Vol. 1.
(16) Wu, C. F.; Zheng, Y. L.; Szymanski, C.; McNeill, J. Energy Transfer in a Nanoscale Multichromophoric System: Fluorescent Dye-Doped Conjugated Polymer Nanoparticles. *J. Phys. Chem. C* **2008**, *112*, 1772−1781.

(17) Wu, C. F.; Peng, H. S.; Jiang, Y. F.; McNeill, J. D. Energy Transfer Mediated Fluorescence from Blended Conjugated Polymer Nanoparticles. *J. Phys. Chem. B* **2006**, *110*, 14148−14154.
(18) Nguyen, T. Q.; Doan, V.; Schwartz, B. J. Conjugated Polymer Aggregates in Solution: Control of Interchain Interactions. *J. Chem. Phys.* **1999**, *110*, 4068−4078.
(19) Schwartz, B. J. Conjugated Polymers as Molecular Materials: How Chain Conformation and Film Morphology Influence Energy Transfer and Interchain Interactions. *Annu. Rev. Phys. Chem.* **2003**, *54*, 141−172.
(20) Huang, B.; Bates, M.; Zhuang, X. W. Super-Resolution Fluorescence Microscopy. *Annu. Rev. Biochem.* **2009**, *78*, 993−1016.
(21) Patterson, G.; Davidson, M.; Manley, S.; Lippincott-Schwartz, J. Superresolution Imaging using Single-Molecule Localization. *Annu. Rev. Phys. Chem.* **2010**, *61*, 345−367.
(22) Widengren, J.; Mets, U.; Rigler, R. Fluorescence Correlation Spectroscopy of Triplet-States in Solution: a Theoretical and Experimental Study. *J. Phys. Chem.* **1995**, *99*, 13368−13379.
(23) Wu, C. F.; Bull, B.; Szymanski, C.; Christensen, K.; McNeill, J. D. Multicolor Conjugated Polymer Dots for Biological Fluorescence Imaging. *ACS Nano* **2008**, *2*, 2415−2423.
(24) Bates, M.; Huang, B.; Dempsey, G. T.; Zhuang, X. W. Multicolor Super-Resolution Imaging with Photo-Switchable Fluorescent Probes. *Science* **2007**, *317*, 1749−1753.
(25) Heilemann, M.; Margeat, E.; Kasper, R.; Sauer, M.; Tinnefeld, P. Carbocyanine Dyes as Efficient Reversible Single-Molecule Optical Switch. *J. Am. Chem. Soc.* **2005**, *127*, 3801−3806.
(26) Tian, Z. Y.; Yu, J. B.; Wang, X. L.; Groff, L. C.; Grimland, J. L.; McNeill, J. D. Conjugated Polymer Nanoparticles Incorporating Antifade Additives for Improved Brightness and Photostability. *J. Phys. Chem. B* **2013**, *117*, 4517−4520.
(27) Van Munster, E. B.; Kremers, G. J.; Adjobo-Hermans, M. J. W.; Gadella, T. W. J. Fluorescence Resonance Energy Transfer (FRET) Measurement by Gradual Acceptor Photobleaching. *J. Microsc.* **2005**, *218*, 253−262.
(28) Eggeling, C.; Widengren, J.; Rigler, R.; Seidel, C. A. M. Photobleaching of Fluorescent Dyes under Conditions used for Single-Molecule Detection: Evidence of Two-Step Photolysis. *Anal. Chem.* **1998**, *70*, 2651−2659.
(29) Plakhotnik, T.; Moerner, W. E.; Palm, V.; Wild, U. P. Single-Molecule Spectroscopy-Maximum Emission Rate and Saturation Intensity. *Opt. Commun.* **1995**, *114*, 83−88.
(30) Bretschneider, S.; Eggeling, C.; Hell, S. W. Breaking the Diffraction Barrier in Fluorescence Microscopy by Optical Shelving. *Phys. Rev. Lett.* **2007**, *98*, 218103-1−218103-4.